American Mineralogist, Volume 68, pages 1059–1075, 1983

Calculation of the thermodynamic and geochemical consequences of nonideal mixing in the system H_2O–CO_2–NaCl on phase relations in geologic systems: metamorphic equilibria at high pressures and temperatures

TERESA SUTER BOWERS[1] AND HAROLD C. HELGESON

Department of Geology and Geophysics
University of California, Berkeley, California 94720

Abstract

Fluid inclusion analyses reported in the literature, together with experimental data and thermodynamic calculations indicate that nonideality in the system H_2O–CO_2–NaCl may have a profound effect on phase relations in metamorphic processes. High concentrations of NaCl in the system H_2O–CO_2–NaCl increase substantially the size of the two-phase (liquid + vapor) region by raising the consolute temperature for a given pressure and ratio of the mole fractions of H_2O and NaCl to more than double that in the binary system H_2O–CO_2. As a consequence, fluid immiscibility may occur at considerable depth during progressive metamorphism of siliceous carbonates. The effect of nonideal mixing of H_2O, CO_2, and NaCl on equilibrium constraints in metamorphic systems can be assessed quantitatively on phase diagrams generated with the aid of a modified Redlich-Kwong equation of state (Bowers and Helgeson, 1983). Diagrams of this kind indicate that increasing NaCl concentration results in higher temperatures and/or lower predicted values of X_{CO_2} for equilibrium mineral assemblages than would be true for the binary system H_2O–CO_2. Transection of various mineral stability fields by saturation lines representing equilibrium between the aqueous phase and calcite, dolomite, or magnesite on logarithmic activity diagrams is also highly sensitive to the NaCl concentration in the aqueous phase. For example, the assemblage tremolite + dolomite + talc coexists with an H_2O-rich fluid at 450°C, 2 kbar, and NaCl concentrations $\leq$1 m. However, as the concentration of NaCl increases to ~4 m, tremolite is no longer stable in the presence of the fluid phase. The slopes of isochores for given bulk compositions in the ternary system H_2O–CO_2–NaCl decrease substantially with increasing CO_2 concentration. The isochores generated from the equation of state for the ternary system can be used to calculate pressure corrections for fluid inclusion homogenization temperatures. Stability fields for certain mineral assemblages in temperature–composition diagrams for the two-phase (liquid + vapor) region of the system H_2O–CO_2–NaCl are much smaller than their counterparts in the one-phase region. Furthermore, all univariant curves which cross the consolute composition curve on such diagrams exhibit temperature minima. These curves terminate in invariant points which are replicated on both sides of the miscibility gap. Subtle changes in NaCl concentration at low to intermediate values of X_{CO_2} may result in the appearance of mineral assemblages commonly thought to occur only in the presence of CO_2-rich fluids. Failure to account for the possible effects of fluid immiscibility on equilibrium mineral assemblages may lead to serious errors in interpretation of phase relations in metamorphic rocks.

Introduction

Considerable evidence indicates that aqueous fluids in a wide range of geologic environments contain significant concentrations of both CO_2 and NaCl. The thermodynamic properties of these fluids have been calculated with the aid of a modified Redlich-Kwong (MRK) equation of state for the ternary system H_2O–CO_2–NaCl (Bowers and Helgeson, 1983). The MRK equation of state was applied to the ternary system by allowing the H_2O parameters in the equation to be functions of NaCl concentration. The equation was then fit to pressure–volume–temperature data reported by Gehrig (1980). The regression parameters derived in this manner were used together with a graphic extrapolation procedure to calculate densities, fugacity coefficients, and the compositions of coexisting

[1] Present address: Division of Geological and Planetary Sciences, California Institute of Technology, Pasadena, California 91125.

0003–004X/83/1112–1059$02.00

phases as a function of pressure at temperatures from 350° to 600°C and concentrations of NaCl from 0 to 35 wt.% NaCl relative to H_2O + NaCl (Bowers and Helgeson, 1983). The purpose of the present communication is to evaluate the effects of compositional variation and immiscibility in H_2O–CO_2–NaCl fluids on mineral equilibria in geochemical processes at high pressures and temperatures. The extent to which such compositional variation and immiscibility occur in hydrothermal systems can be assessed with the aid of fluid inclusion data.

Studies of fluid inclusions in quartz and feldspar in granitic rocks from trachytic breccias on Ascension Island (Roedder and Coombs, 1967) indicate that a 60–70 wt.% NaCl fluid unmixed to form an H_2O-rich liquid and a CO_2-rich vapor between ~550° and 700°C. Unmixing also apparently occurred in fluid inclusions studied by Roedder (1971) in the porphyry ores at Bingham, Utah, between 400° and 700°C. The liquid in these inclusions contains up to 60 wt.% salts and the CO_2-rich vapor phase contains 6–7 wt.% salts. In contrast, Barton *et al.* (1977), in a study of the environment of ore deposition in the Creede Mining District, Colorado, cite fluid inclusion evidence for the unmixing of a 1 molal NaCl fluid to produce a CO_2-rich vapor at ~270°C and 50 bars. Leroy and Poty (1969) and Poty *et al.* (1974) detected a large range of X_{CO_2}/X_{H_2O} (where X_{CO_2} and X_{H_2O} designate the mole fractions of CO_2 and H_2O, respectively) in a series of fluid inclusions in the uranium deposits in the Saint-Sylvestre granite in the Central Massif in France. Immiscibility apparently occurred in these inclusions at ~340–350°C and 700–800 bars. They suggest that the concentration of uranium in solution is closely related to the CO_2 content, and that the uranium is possibly being transported as uranyl carbonate complexes. They further postulate that with decreasing pressure and concomitant unmixing of the fluid phase, the complexes dissociate, causing uranium to precipitate. Similar observations and postulates have been made by Lyakhov and Popivnyak (1978) and Petrovskaya *et al.* (1973) in gold deposits in Northern Buryatia, the Lena region, and several other locations in the Soviet Union. Analyses of fluid inclusions in quartz in the gold–quartz veins in these regions reveal variable amounts of CO_2 and a wide range of homogenization temperatures, indicating fluid immiscibility. However, these characteristics are not observed in fluid inclusions in the nonproductive zones. Petrovskaya *et al.* (1973) note that periodic unmixing of the solutions could have been caused by abrupt decreases in pressure at the openings of fissure cavities where the ore deposits formed. Lyakhov and Popivnyak observe maximum immiscibility in fluid inclusions with homogenization temperatures of 210–260°C. They suggest that the pressure drop and associated degassing of the gold-bearing solutions may have contributed to the breakdown of the complexes responsible for transporting the gold.

Three recent studies of fluid inclusions indicate that regions of fluid immiscibility in metamorphic systems may extend well beyond those exhibited by the binary system H_2O–CO_2. Examination of fluid inclusions in matrix quartz crystals from an area of high-grade amphibolite facies in the Khtada Lake region in British Columbia (Hollister and Burruss, 1976) indicates that separation of an H_2O-rich liquid and a CO_2-rich vapor occurred at temperatures at least 75°C in excess of high-pressure consolute temperatures in the binary system H_2O–CO_2. Approximately 5–6 wt.% NaCl is present in the H_2O-rich liquid in these inclusions. Similarly, Hendel and Hollister (1981) demonstrated by plotting homogenization temperatures as a function of the mole fraction of CO_2 that immiscibility occurred in fluid inclusions containing 2.6 wt.% NaCl relative to H_2O + NaCl in quartz veinlets in a pelitic schist at temperatures ~65°C higher than the consolute temperatures for pressures between 1 and 2 kbar in the system H_2O–CO_2. In addition, Sisson *et al.* (1981) describe fluid inclusions in quartz segregations in a calcareous psammite and a carbonate schist which exhibit immiscibility between a brine containing ~24 wt.% dissolved solids and a CO_2-rich vapor at 600°C and 6.5 kbar.

The observations summarized above leave little doubt that both NaCl and CO_2 may be present in high concentrations in crustal fluids, and that these fluids may unmix at high temperatures and pressures. Nevertheless, pressure corrections applied to fluid inclusion homogenization temperatures are commonly calculated by assuming that the pressure–volume–temperature properties of the fluids in the inclusions can be approximated closely by those of pure H_2O. However, even small amounts of CO_2 or NaCl may alter substantially these properties. The effect of such differences on pressure corrections of fluid inclusion homogenization temperatures can be assessed with the aid of the MRK equation of state adduced above.

Pressure corrections for homogenization temperatures of fluid inclusions in the ternary system H_2O–CO_2–NaCl

Calculated densities of fluids in the ternary system H_2O–CO_2–NaCl (Bowers and Helgeson, 1983) are shown as isochores on the pressure–temperature diagrams depicted in Figures 1–5. The solid curves in Figure 1 represent pure H_2O, which is designated A in the composition diagram in the upper left corner of the figure. The dashed curves refer to H_2O–CO_2 fluids containing 10 mole% CO_2 (solution B). The dot-dash curves correspond to H_2O–CO_2–NaCl fluids with 10 mole% CO_2 and 1.74 mole% NaCl (solution C). Although fluid inclusions containing pure H_2O homogenize along the equilibrium vapor-liquid saturation curve for the system H_2O shown in Figure 1, those with compositions corresponding to solutions B and C homogenize along the curves labeled D and E, respectively. Certain areas in the figure are shaded or hachured to emphasize the shift in the slopes of the isochores resulting from addition of CO_2 and NaCl. This effect is most pronounced at high temperatures.

The isochores depicted in Figures 2–5 refer to the bulk compositions labeled A through P in Figure 6A. The dashed curves represent the limits of the two-phase vapor + liquid immiscible region extrapolated from published experimental solubility data by Bowers and Helgeson (1983).[2] Note in these figures that the slopes of the isochores decrease only slightly with increasing NaCl concentration at constant X_{CO_2} (diagrams A–D in Fig. 2), but they decrease dramatically with increasing X_{CO_2} at constant X_{NaCl} (diagrams B,F,J,L,N, and P in Figs. 2–5). It can be seen that the limits of the two-phase region shift to higher temperatures with increasing NaCl concentration.

The diagrams shown in Figures 2–5 can be used to calculate pressure corrections for fluid inclusion homogenization temperatures if the fluid composition is known. Isochores for bulk compositions not shown in these figures can be generated from densities taken from tables or calculated from the MRK equation of state for the ternary system H_2O–CO_2–NaCl given by Bowers and Helgeson (1983).

Phase relations among minerals and H_2O–CO_2–NaCl fluids

Jacobs and Kerrick (1981) have demonstrated experimentally that compositional variation of fluids in the ternary system H_2O–CO_2–NaCl may affect significantly mineral equilibria in metamorphic systems.[3] Several examples of these effects on dehydration and decarbonation reactions are discussed below. The thermodynamic properties of minerals and H_2O employed in the calculations were generated from equations and data summarized by Helgeson and Kirkham (1974), Helgeson *et al.* (1978), and Helgeson *et al.* (1981). Fugacities of H_2O and CO_2 were calculated from the MRK equation of state for the ternary system H_2O–CO_2–NaCl using parameters generated by Bowers and Helgeson (1983).

Dehydration reactions

Univariant curves representing equilibria among minerals and a fluid phase are shown in Figure 7. The coexistence of muscovite and quartz with andalusite, K-feldspar, and a fluid is depicted in Figure 7A for various values of X_{CO_2} along binary PA-1 in Figure 6B. The curves in Figure 7B refer to fluid compositions along parabinary PA-2 in Figure 6B. Those in Figure 7C are for constant $X_{CO_2} = 0.1$ and the designated values of X_{NaCl}, which correspond approximately to molalities of 0, 1, 2,

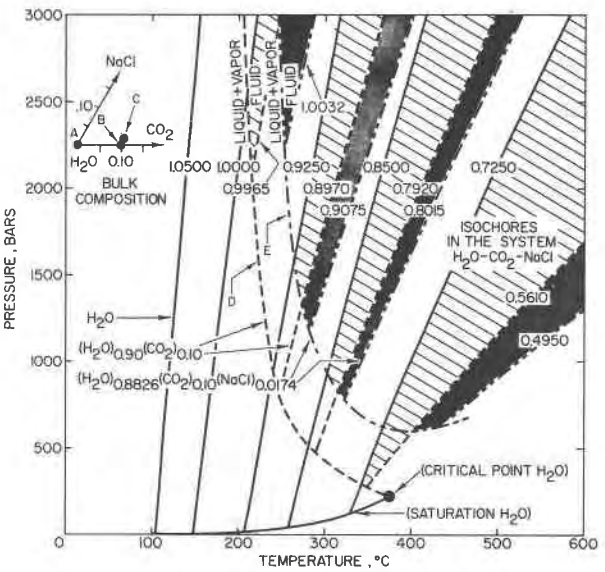

Fig. 1. Isochores (designated in g cm^{-3}) for solution compositions corresponding to pure H_2O (solid curves), 90 mole% H_2O and 10 mole% CO_2 (dashed curves), and 88.26 mole% H_2O, 10 mole% CO_2, and 1.74 mole% NaCl (double dot-dash curves)—see text.

and 4, respectively. The long-dash curves in Figure 7 represent metastable extensions of the equilibrium curves into the sillimanite or kyanite stability fields. The short-dash curves in Figures 7B and C represent the limits of the two-phase vapor + liquid immiscible region in the ternary system H_2O–CO_2–NaCl.

The equilibrium assemblage represented by the curves in Figure 7 consists of six components and five coexisting phases in the fluid-phase region of the subsystem H_2O–CO_2–NaCl. Of the three degrees of freedom required by the phase rule, two are constrained by specifying the concentration of CO_2 and NaCl in the fluid, which results in the isocompositional univariant curves shown in the diagrams. The intersection of these curves with the boundary of the two-phase liquid + vapor region in the system H_2O–CO_2–NaCl is thus invariant at constant composition. Note that addition of CO_2 and/or NaCl at a given pressure lowers significantly the equilibrium temperature for the dehydration reaction.

Equilibria in the system CaO–MgO–SiO_2–H_2O–CO_2–NaCl

Phase relations in this system at 2 kbar are shown in Figures 8–13 as a function of temperature and X_{CO_2} or N_{CO_2}, which is defined by[4]

$$N_{CO_2} \equiv \frac{R_{CO_2}}{R_{CO_2} + 1} \quad (1)$$

[2] The terms liquid and vapor are used in the present communication to designate coexisting phases of higher and lower densities, respectively, in an immiscible region of pressure–temperature–composition space. The term fluid is used to designate a single phase.

[3] For the most part, Jacobs and Kerrick's (1981) experimental data compare favorably with fluid compositions calculated from the MRK equation of state (Bowers and Helgeson, 1983).

[4] N_{CO_2} in the present communication corresponds to N_{CO_2/H_2O} in Bowers and Helgeson (1983).

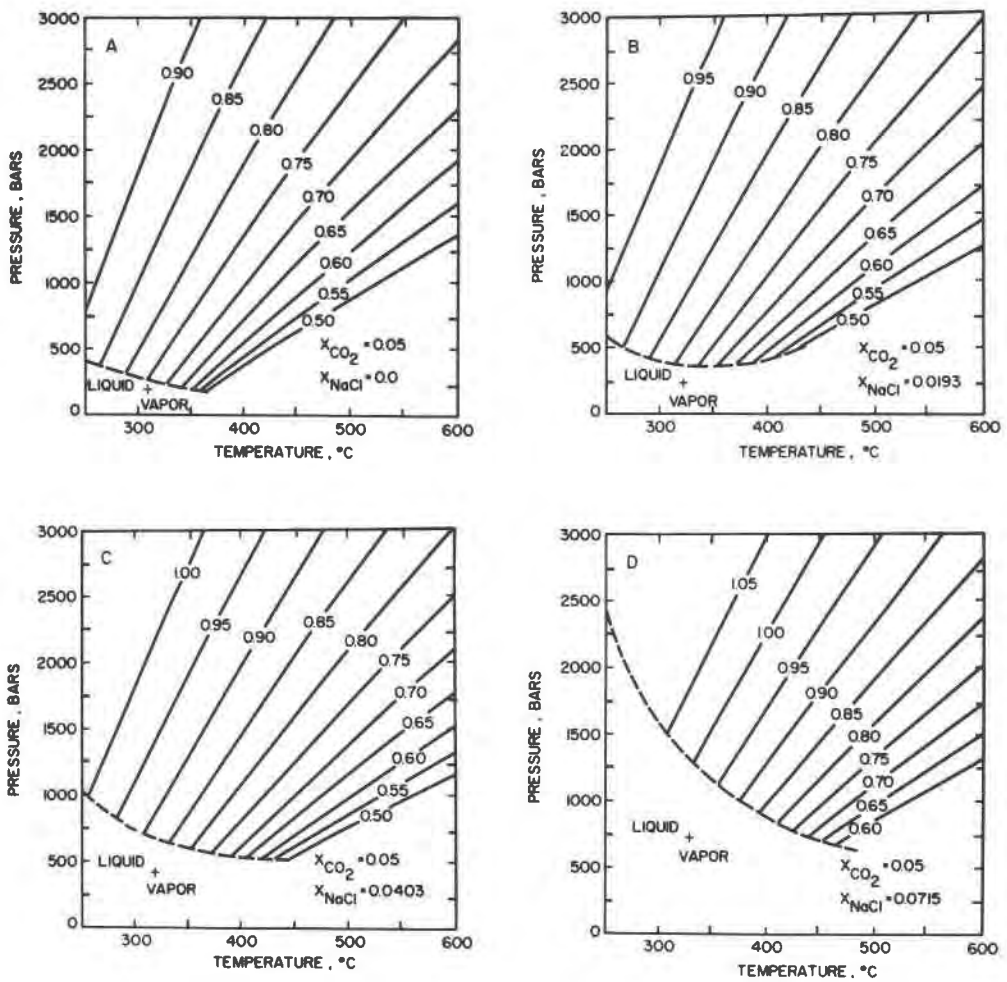

Fig. 2. Isochores (solid curves, designated in g cm^{-3}) for fluids with the bulk compositions labeled in the lower right corner of each diagram. The letters in the upper left corners correspond to the same letters shown in Fig. 6A. The dashed curves represent the limits of the miscibility gap in the system H_2O–CO_2–NaCl.

where

$$R_{CO_2} \equiv \frac{X_{CO_2}}{X_{H_2O}} . \quad (2)$$

Note that only for the binary system H_2O–CO_2 is N_{CO_2} equal to X_{CO_2}. The circled letters shown in Figures 8, 12, and 13 designate fluid compositions and temperatures represented by activity diagrams presented below.

Figure 8 (Walther and Helgeson, 1980) refers to the H_2O–CO_2 binary, but Figures 9 and 10 represent phase relations along the pseudobinaries through the ternary system H_2O–CO_2–NaCl designated as PS-1 and PS-2 in Figure 6C. It can be seen in Figure 9 that the miscibility gap in the system H_2O–CO_2–NaCl at 2 kbar occupies only a small part of temperature–X_{CO_2} space above 400°C along PS-1. As a consequence, none of the curves representing mineral equilibria intersects the miscibility gap in Figure 9. Nevertheless, it can be deduced by comparison of Figures 8 and 9 that increasing departures from ideality in the fluid with increasing NaCl concentration result in higher equilibrium temperatures for reactions at low X_{CO_2}. This effect diminishes with increasing X_{CO_2}.

Invariant point A in Figure 8, which represents the assemblage talc, dolomite, calcite, quartz, tremolite, and fluid is displaced to A′ in Figure 9. The fluid composition represented by A in Figure 8 corresponds to that designated A in Figure 9. Note that the difference between A and A′ is ~4 mole% CO_2, which is of the order of the maximum difference in the positions of corresponding curves in the H_2O-rich regions of Figures 8 and 9.

In contrast to Figure 9, the miscibility gap in the system H_2O–CO_2–NaCl is a prominent feature of Figure 10, where the consolute temperature reaches ~535°C. As a consequence, seven new invariant points occur in the diagram. It should perhaps be emphasized that curves such as those representing equilibrium among talc, for-

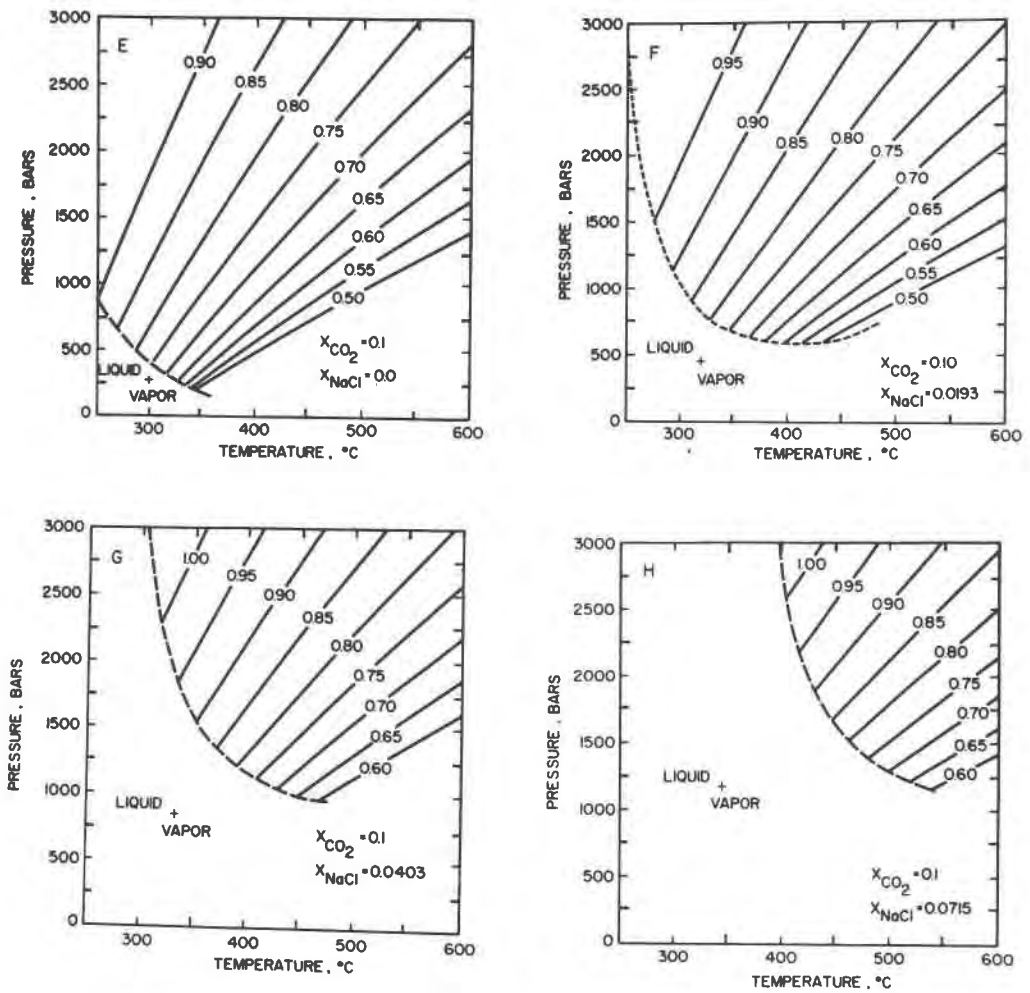

Fig. 3. Isochores (solid curves, designated in g cm^{-3}) for fluids with the bulk compositions labeled in the lower right corner of each diagram. The letters in the upper left corners correspond to the same letters shown in Fig. 6A. The dashed curves represent the limits of the miscibility gap in the system H_2O–CO_2–NaCl.

sterite, magnesite, and the fluid phase in Figure 10 terminate in invariant points at different temperatures on either side of the miscibility gap. The temperature difference occurs because pseudobinary PS-2 in Figure 6C does not coincide with any of the equilibrium tie lines shown in Figure 6D. As a consequence, no tie lines can be drawn through the miscibility gap on the plane represented by Figure 10. Similarly, no curve is shown connecting corresponding invariant points on either side of the miscibility gap because the compositions of the coexisting vapor and liquid phases in this region do not fall on the plane of the paper.

The invariant point labeled A and A′ in Figures 8 and 9, respectively, does not appear in Figure 10 because the figure refers to a fixed value of X_{NaCl}/X_{H_2O} and the equilibrium assemblage talc, dolomite, calcite, quartz, and tremolite occurs together with both a liquid and vapor phase along a tie line within the immiscible region of the system H_2O–CO_2–NaCl. This can be seen in the schematic three-dimensional diagram in Figure 11, where two of the curves that meet at invariant point A and A′ in Figures 8 and 9 are represented by surfaces in temperature–X_{CO_2}–X_{NaCl} space. The surface bounded by AA′B′BFC in Figure 11 represents

$$\underset{\text{(dolomite)}}{3CaMg(CO_3)_2} + \underset{\text{(quartz)}}{4SiO_2} + H_2O = \underset{\text{(talc)}}{Mg_3Si_4O_{10}(OH)_2} + \underset{\text{(calcite)}}{3CaCO_3} + 3CO_2 \quad (3)$$

and surfaces AA′D′D and BB′E′E correspond to

$$\underset{\text{(dolomite)}}{2CaMg(CO_3)_2} + \underset{\text{(talc)}}{Mg_3Si_4O_{10}(OH)_2} + \underset{\text{(quartz)}}{4SiO_2} = \underset{\text{(tremolite)}}{Ca_2Mg_5Si_8O_{22}(OH)_2} + 4CO_2 \quad (4)$$

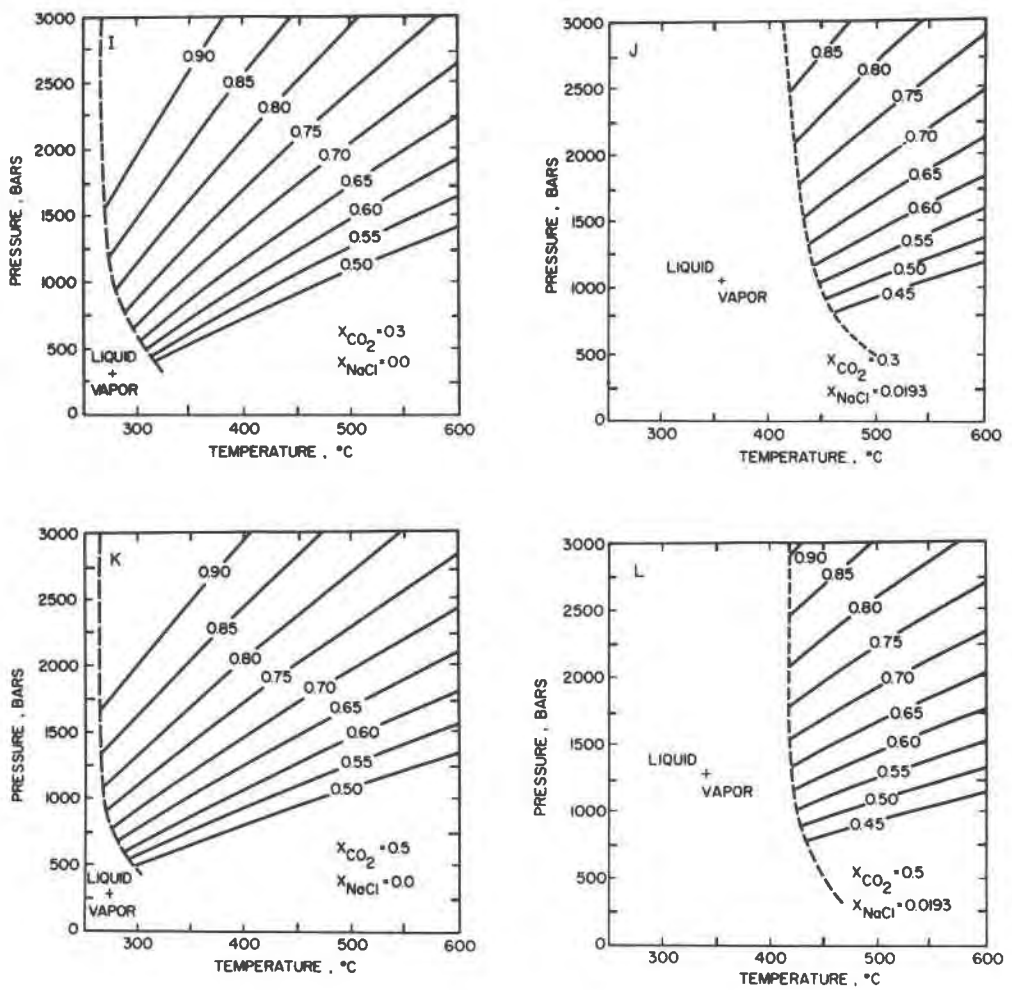

Fig. 4. Isochores (solid curves, designated in g cm^{-3}) for fluids with the bulk compositions labeled in the lower right corner of each diagram. The letters in the upper left corners correspond to the same letters shown in Fig. 6A. The dashed curves represent the limits of the miscibility gap in the system H_2O–CO_2–NaCl.

Curves AC and AD in Figure 11 correspond to univariant curves in the plane of the H_2O–CO_2 binary depicted in Figure 8. The miscibility gap in the system H_2O–CO_2–NaCl is bounded in Figure 11 by D′A′B′E′JH.

Univariant curves on phase diagrams like those shown in Figures 8–10, 12, and 13 correspond to the intersection of pseudobinary or parabinary planes with divariant surfaces like those in Figure 11. Invariant points such as A in Figure 8 become univariant curves (AA′) in the one-phase region of the ternary system (Fig. 11). Note that where a univariant curve like AA′ (which corresponds to the coexistence of talc, dolomite, calcite, quartz, tremolite, and fluid) intersects the miscibility gap (at A′) the curve terminates in an invariant point which is replicated on the opposite side of the immiscible region (at B′). As a consequence, the invariant assemblage is stable for all bulk compositions along the tie line connecting A′ and B′ in the immiscible region. The intersection of this tie line (as well as the other tie lines shown in Figure 11) with the pseudobinary represented by Figure 10 is not shown in the latter figure because the compositions of the coexisting vapor and liquid phases do not fall on the plane of the diagram.

Univariant curve BB′ in Figure 11 corresponds to the analog of AA′ in the liquid phase region. The assemblage tremolite + liquid + vapor is stable at temperatures above those corresponding to surface D′A′B′E′ in Figure 11, which consists of liquid-vapor tie lines. At temperatures below those represented by this surface, the assemblage dolomite + talc + quartz + liquid + vapor is stable. At more H_2O-rich bulk compositions, talc, calcite, liquid, and vapor coexist at temperatures above those corresponding to A′B′A′, but dolomite, talc, quartz, liquid, and vapor are in equilibrium below the tie line surface denoted by A′B′A′. This trivariant phase region above the tie line surface is bounded at higher temperatures by a

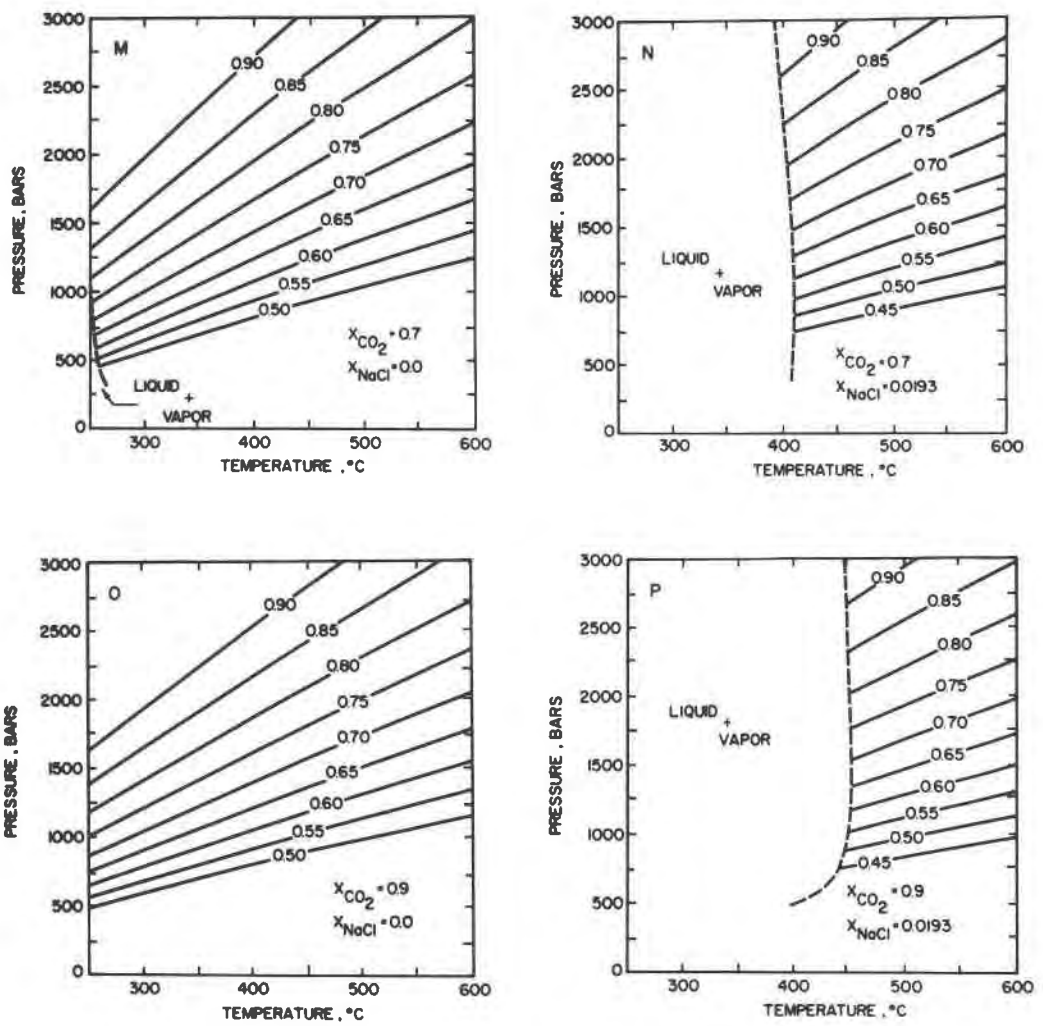

Fig. 5. Isochores (solid curves, designated in g cm^{-3}) for fluids with the bulk compositions labeled in the lower right corner of each diagram. The letters in the upper left corners correspond to the same letters shown in Fig. 6A. The dashed curves represent the limits of the miscibility gap in the system H_2O–CO_2–NaCl.

divariant surface corresponding to equilibrium among talc, calcite, quartz, tremolite, liquid, and vapor, which extends from the limits of the immiscible region at higher temperatures to tie line A′B′. This surface, as well as other surfaces represented by univariant curves in Figures 8 through 10 were omitted from Figure 11 for the sake of clarity.

Figures 12 and 13 correspond to parabinaries through the one-phase region of the ternary system H_2O–CO_2–NaCl along PA-2 and PA-3 in Figure 6B, respectively. It should be emphasized that the positions of the invariant points shown in Figure 13 are somewhat uncertain because they lie outside of the compositional region represented by the experimental data array used to generate the regression parameters in the MRK equation of state. As a consequence, fugacity coefficients had to be extrapolated (Bowers and Helgeson, 1983) to calculate these fluid compositions. The parabinary phase diagrams shown in Figures 12 and 13 do not differ significantly from their pseudobinary counterparts in Figures 9 and 10, but they are perhaps more geologically relevant because they represent fluids with constant concentrations of NaCl.

Activity diagrams are shown in Figure 14, which refer to the fluid compositions and temperatures represented by the circled letters in Figures 8, 12, and 13. The symbols $\sigma_{Mg^{++}}$ and $\sigma_{Ca^{++}}$ stand for solvation parameters defined by (Walther and Helgeson, 1980)

$$\sigma_i \equiv a_{H_2O}^{(n_i - Z_i n_{H^+})} \tag{5}$$

where n_i and Z_i refer to the solvation number and charge of the ith aqueous species. The dashed lines on the activity diagrams represent fluid saturation with respect to calcite (horizontal lines), magnesite (vertical lines), and dolomite (diagonal lines). Regions of the diagrams

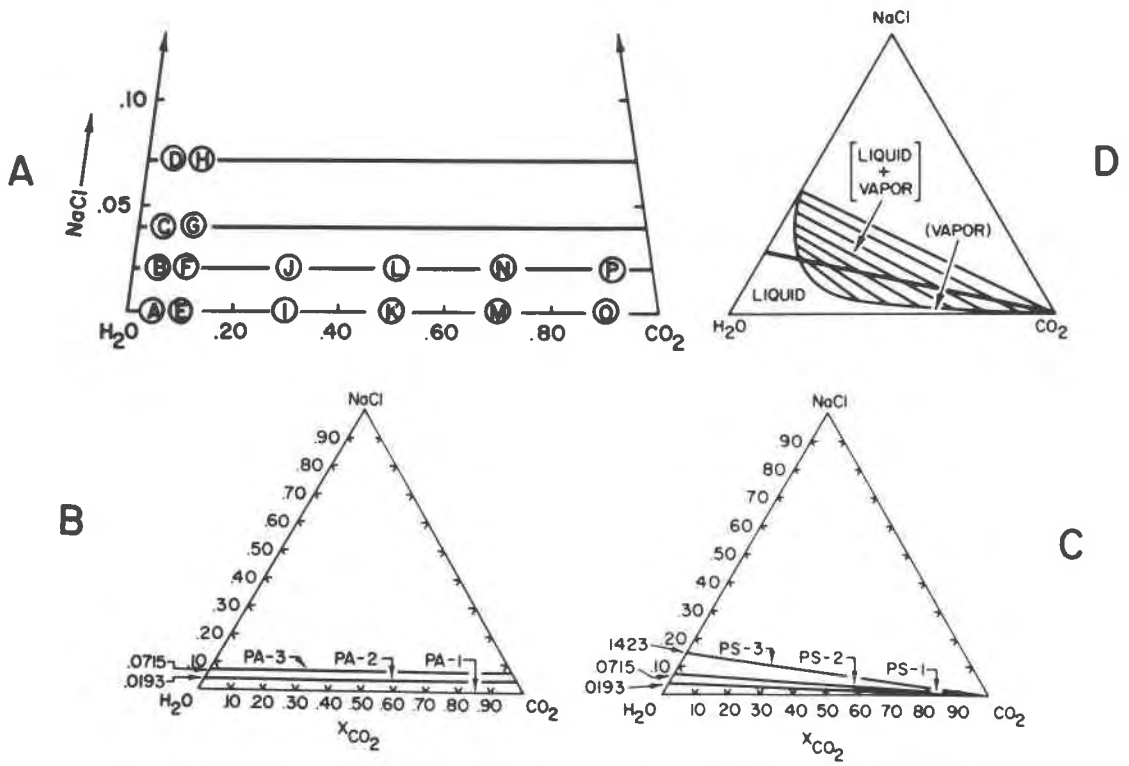

Fig. 6. Diagram A: Bulk compositions in the ternary system H_2O–CO_2–NaCl designated by letters A–P in Figures 2–5. Diagram B: Bulk compositions corresponding to binary PA-1 and parabinaries PA-2 and PA-3, for which X_{NaCl} = 0, 0.0193 and 0.0715, respectively. Diagram C: Bulk compositions in the ternary system corresponding to pseudobinaries PS-1, PS-2, and PS-3 for which N_{NaCl} = 0.0193, 0.0715, and 0.1423. Diagram D: Schematic phase diagram for the ternary system H_2O–CO_2–NaCl at a given temperature and pressure (see text).

corresponding to values of $\log(a_{Mg^{++}}/(\sigma_{Mg^{++}}a^2_{H^+}))$ and $\log(a_{Ca^{++}}/(\sigma_{Ca^{++}}a^2_{H^+}))$ that are greater than those corresponding to the dashed saturation lines represent metastable equilibria.

It can be deduced from Figures 8, 12, and 13, together with the activity diagrams designated B, D, and F in Figure 14 that the tremolite stability field in the presence of calcite, dolomite, and a fluid phase becomes smaller and disappears with increasing NaCl concentration at 450°C and N_{CO_2} = 0.05. Similarly, it can be deduced from Figures 8, 12, 13, and the activity diagrams annotated C, E, and G in Figure 14 that forsterite becomes metastable in the presence of a fluid phase at 500°C, N_{CO_2} = 0.10, and concentrations of NaCl in excess of $X_{NaCl} \approx 0.02$.

Phase relations in the system CaO–MgO–SiO_2–H_2O–CO_2–NaCl at 2 kbar and 500°C are depicted in Figure 15 in terms of N_{CO_2} and either $\log(a_{Mg^{++}}/(\sigma_{Mg^{++}}a^2_{H^+}))$ or $\log(a_{Ca^{++}}/(\sigma_{Ca^{++}}a^2_{H^+}))$. Figure 15A, which refers to X_{NaCl} = 0 (PA-1 in Figure 6B) was taken from Walther and Helgeson (1980). Figures 15B and 15C refer to parabinary PA-2 in Figure 6B (X_{NaCl} = 0.0193), but Figure 15D represents parabinary PA-3 (X_{NaCl} = 0.0715). The positions of the invariant points shown in Figure 15D are somewhat uncertain because extrapolated fugacity coefficients were used to calculate the fluid compositions (Bowers and Helgeson, 1983). Nevertheless, it can be seen by comparing Figures 15A through D that the invariant points occur at lower N_{CO_2} values with increasing NaCl concentration.

Phase relations among minerals, liquid, and vapor in the two-phase region of the ternary system H_2O–CO_2–NaCl

Correlation of pressure–volume–temperature relations for the ternary system H_2O–CO_2–NaCl with temperatures, pressures, and bulk fluid compositions characteristic of metamorphic terranes (Sisson *et al.*, 1981; Hendel and Hollister, 1981; Kreulen, 1980; Crawford *et al.*, 1979; Hollister and Burruss, 1976; among others) indicates that fluid immiscibility may occur far more commonly in metamorphic processes than has been generally recognized in the past. Because the presence of coexisting liquid and vapor has a dramatic effect on equilibrium temperatures for dehydration and decarbonation reactions, failure to take into account the thermodynamic consequences of vapor-liquid immiscibility may lead to serious errors in interpreting phase relations in metamorphic rocks. This can be demonstrated by comparing the

temperature–X_{CO_2} diagram in Figure 8 (for which X_{NaCl} = 0) with the corresponding temperature–N_{CO_2} diagram in Figure 16, which represents equilibrium among minerals in the system CaO–MgO–SiO_2–H_2O–CO_2 in the presence of both liquid and vapor in the two-phase immiscible region of the system H_2O–CO_2–NaCl.

The curves shown in Figure 16 represent projections from X_{NaCl} = 1 of phase relations on the face of the miscibility gap (which corresponds to the surface bounded by D'A'B'E'JH in Figure 11) to a temperature–N_{CO_2} plane at X_{NaCl} = 0. As a consequence, the mineral stability fields shown in the figure correspond to those in the two-phase region of the ternary system H_2O–CO_2–NaCl. Note that each of the univariant curves and invariant points on the CO_2-rich side of the miscibility gap in Figure 16 are repeated on the H_2O-rich side. Each corresponding curve or invariant point can be connected by an isothermal tie line, along which the indicated mineral assemblages are stable in the immiscible region. For example, invariant points A and B in Figure 16, which represent the coexistence of talc, dolomite, calcite, quartz, tremolite, liquid, and vapor correspond to invariant points A' and B' in Figure 11, which are connected by a tie line. Similarly, a given point on a univariant curve on the CO_2-rich side of the miscibility gap, such as *b'*, can be connected by an isothermal tie line to its H_2O-rich counterpart (*b*) as shown in Figure 17. All but a few such tie lines have been omitted from Figure 16 for the sake of clarity, but an example is shown in Figure 17, where the stable mineral assemblages coexisting with liquid + vapor at 525°C are shown along cross section *ff'* in Figure 16. The letters shown within the large circles in Figure 17 denote the limits in the large triangle of the compositional range of liquid + vapor for which the assemblages designated in the circled triangles are stable. The letters in the large triangular cross section in Figure 17 designate the intersections of univariant curves with the line of the cross section in Figure 16.

It can be deduced from Figure 17 that calc-silicate compatibilities in the two-phase liquid + vapor region of the system H_2O–CO_2–NaCl are highly sensitive to small differences in NaCl concentration. For example, increasing X_{NaCl} at N_{CO_2} = 0.5 from 0.166 by only 0.003 to 0.169 changes the stable mineral assemblage from that represented by *bb'c'c* to that designated as *cc'd'd*. Because of the dual occurrence of each invariant point in Figure 16, the mineral assemblages coexisting with liquid and vapor in regions such as *cc'd'd* in Figure 17 are stable at any given temperature over a wide range of bulk compositions in the system H_2O–CO_2–NaCl. *Note that in the absence of high enough NaCl concentrations to cause immiscibility, all of the univariant curves and invariant points on the H_2O-rich side of the phase diagram shown in Figure 16 occur at equivalent temperatures and pressures only in the presence of a single CO_2-rich fluid phase.* It follows that fluid inclusion analyses are a requisite for reliable interpretation of metamorphic phase assemblages.

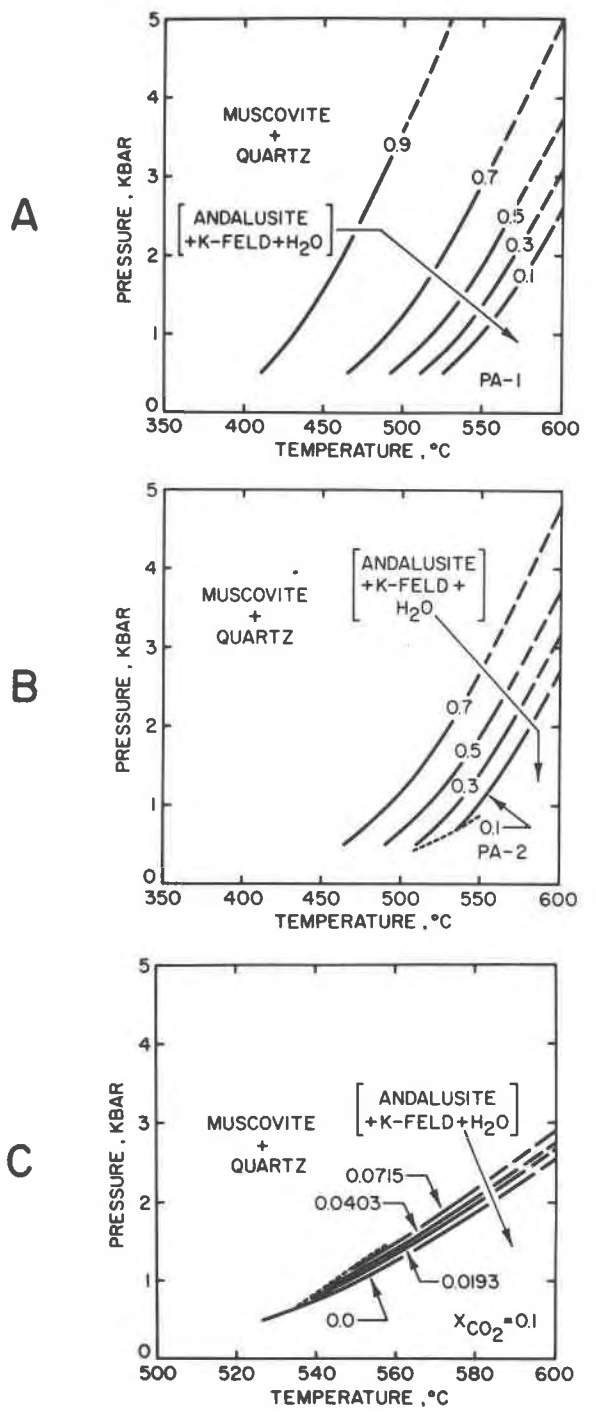

Fig. 7. Diagram A: Univariant dehydration curves for fluid compositions along the H_2O–CO_2 binary designated PA-1 in Fig. 6B. Diagram B: univariant dehydration curves for fluid compositions along parabinary PA-2 in Fig. 6B. The labels on the curves correspond to values of X_{CO_2}. Diagram C: Univariant dehydration curves for fluid compositions with constant X_{CO_2} = 0.1. The labels on the curves correspond to values of X_{NaCl}, and the short-dash curves represent the limits of the miscibility gap in the system H_2O–CO_2–NaCl (see text).

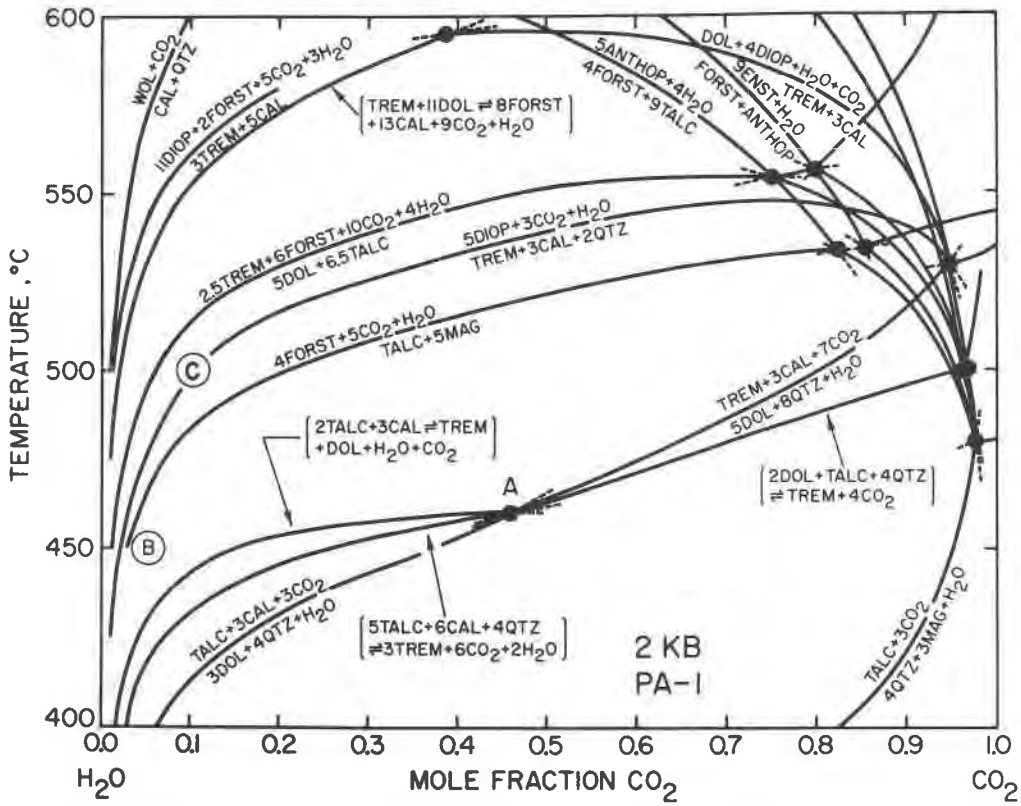

Fig. 8. Temperature–X_{CO_2} diagram depicting mineral–fluid equilibria in the system CaO–MgO–SiO_2–H_2O–CO_2 at 2 kbar taken from Walther and Helgeson (1980). The circled letters designate temperatures and fluid compositions represented by activity diagrams in Fig. 14. CAL = calcite, DOL = dolomite, QTZ = quartz, TREM = tremolite, FORST = forsterite, DIOP = diopside, MAG = magnesite, WOL = wollastonite, ANTHOP = anthophyllite, and ENST = enstatite.

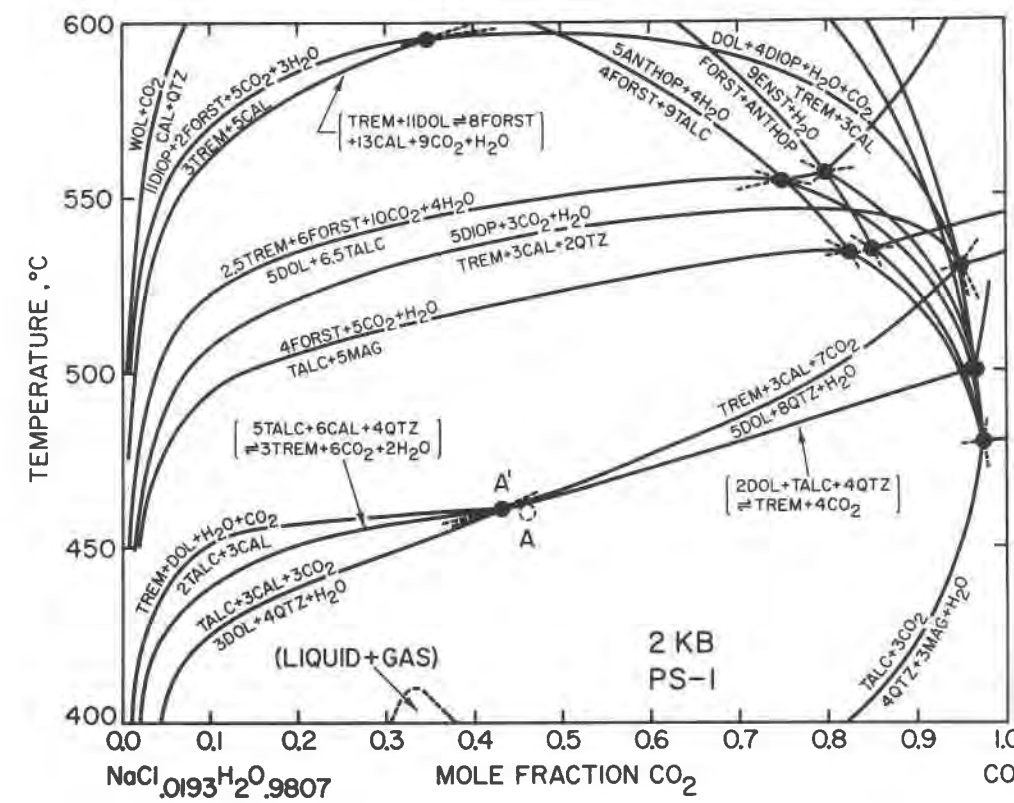

Fig. 9. Temperature–X_{CO_2} diagram depicting mineral–fluid equilibria in the system CaO–MgO–SiO_2–H_2O–CO_2–NaCl at 2 kbar along pseudobinary PS-1 in Fig. 6C. The dotted invariant point A corresponds to invariant point A in Fig. 8 (see text and caption of Fig. 8).

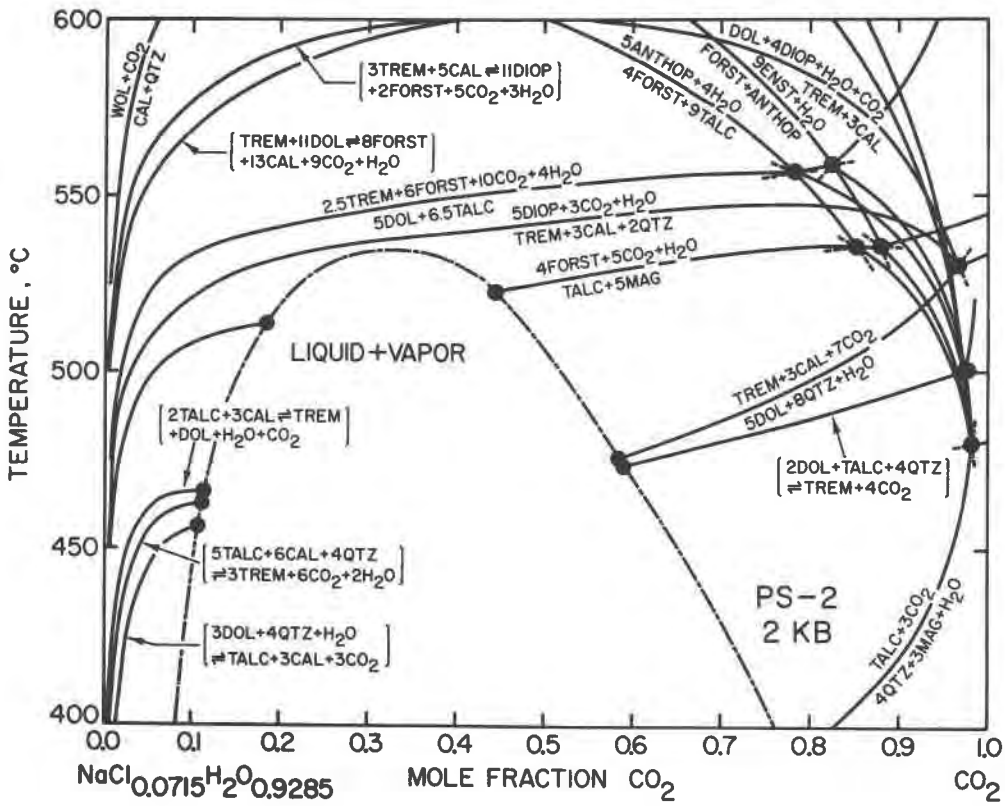

Fig. 10. Temperature–X_{CO_2} diagram depicting mineral–fluid equilibria in the system CaO–MgO–SiO_2–H_2O–CO_2–NaCl at 2 kbar along pseudobinary PS-2 in Fig. 6C. The dot–dash curve represents the limits of the miscibility gap in the system H_2O–CO_2–NaCl (see text and caption of Fig. 8).

All of the curves in Figure 16 that cross over the consolute composition curve for the system H_2O–CO_2–NaCl exhibit minima along the face of the miscibility gap. The minima result from the intersection of the miscibility gap with the divariant surfaces representing the equilibrium phase assemblages in temperature–X_{NaCl}–N_{CO_2} space. In certain cases these minima restrict significantly the range of temperature and N_{CO_2} over which a given mineral assemblage is stable in the immiscible region. For example, it can be seen in Figure 16 that immiscibility causes the univariant curves representing both liquid and vapor coexisting with (1) dolomite, quartz, talc, and calcite, (2) talc, calcite, quartz, and tremolite, and (3) talc, calcite, tremolite, and dolomite to exhibit temperature minima between $N_{CO_2} = 0.2$ and $N_{CO_2} = 0.25$. As a consequence, the sizes of the stability fields between these curves are drastically reduced from their counterparts for $X_{NaCl} = 0$ in Figure 8. Note that as a result of increasing X_{NaCl} and concomitant fluid immiscibility, each of the curves in Figure 8 that exhibits a maximum is represented by a corresponding curve in Figure 16 that exhibits two maxima, one each at high and low values of N_{CO_2}. As a result, mineral assemblages that would otherwise be stable only at low temperatures in the presence of an H_2O-rich fluid occur at much higher temperatures in the presence of coexisting liquid and vapor phases.

The effects of immiscibility in the system H_2O–CO_2–

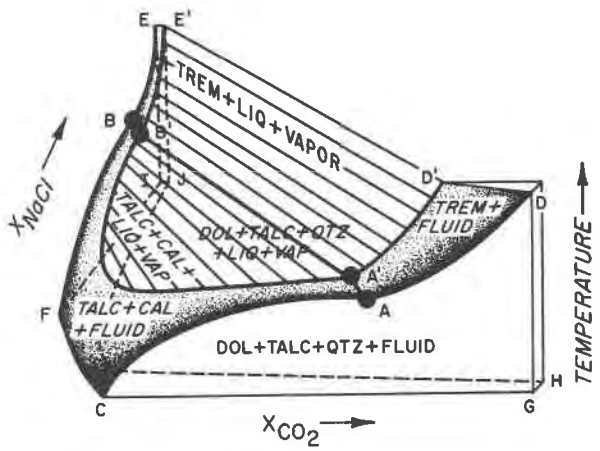

Fig. 11. Schematic 3-dimensional representation of phase relations in the system CaO–MgO–SiO_2–H_2O–CO_2–NaCl at 2 kbar (see text and caption of Fig. 8).

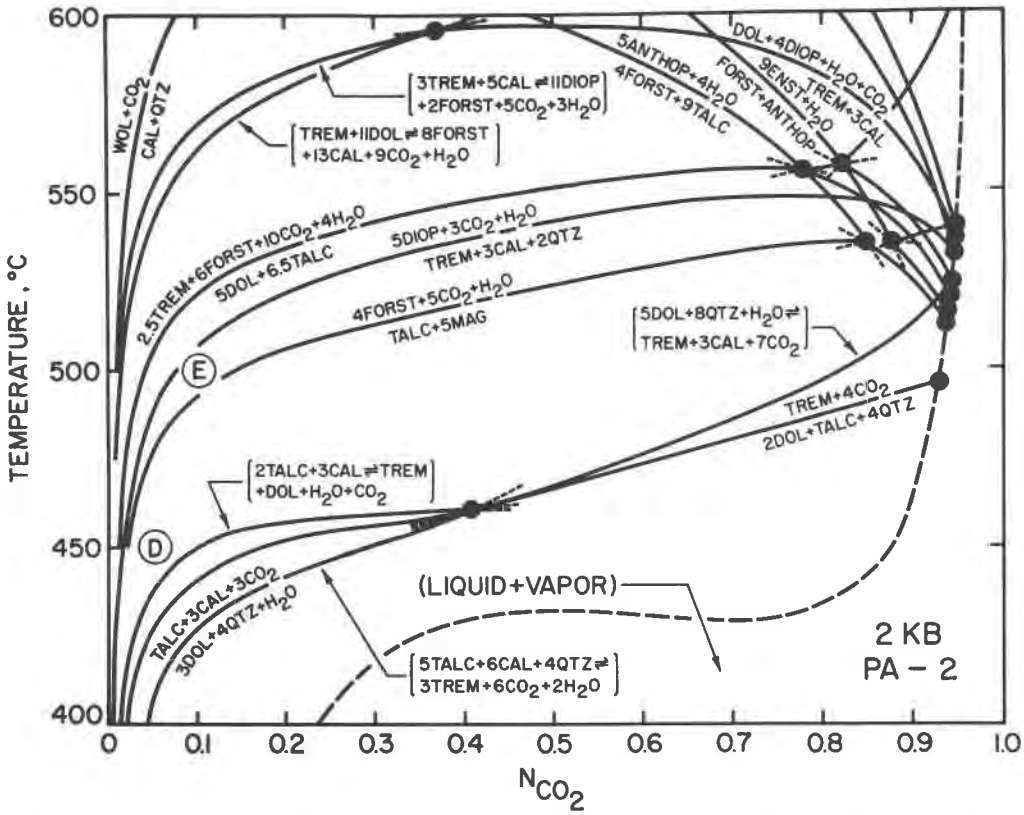

Fig. 12. Temperature–N_{CO_2} diagram depicting mineral–fluid equilibria in the system CaO–MgO–SiO_2–H_2O–CO_2–NaCl at 2 kbar along parabinary PA-2 in Fig. 6B. The long-dash curve represents the limits of the miscibility gap in the system H_2O–CO_2–NaCl (see text and caption of Fig. 8).

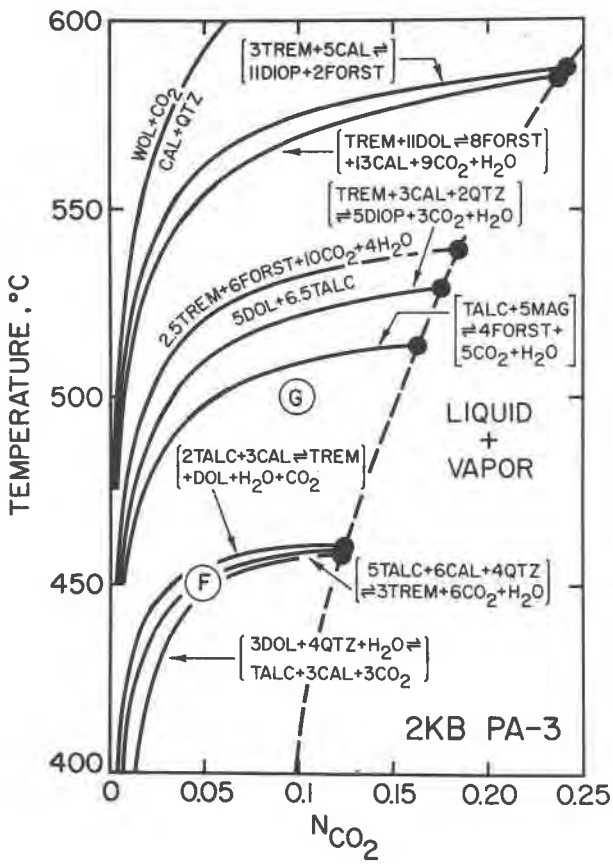

NaCl on the activity ratios of ionic species characteristic of mineral equilibria in the system CaO–MgO–SiO_2–H_2O–CO_2 can be assessed in Figure 18, where $\log(a_{Mg^{++}}/(\sigma_{Mg^{++}}a_{H^+}^2))$ is plotted as a function of N_{CO_2} in a projection from $X_{NaCl} = 1$ of phase relations on the face of the miscibility gap at 500° and 2 kbar to an $N_{CO_2} - \log(a_{Mg^{++}}/(\sigma_{Mg^{++}}a_{H^+}^2))$ plane at $X_{NaCl} = 0$. Tie lines (which are not shown for the sake of clarity) can be drawn to connect points of equal $\log(a_{Mg^{++}}/(\sigma_{Mg^{++}}a_{H^+}^2))$ on either side of the miscibility gap in Figure 18. As in the case of Figure 16, each invariant point appears on opposite sides of the consolute composition curve. Comparison of Figures 15C and 18 indicates that immiscibility introduces minima in the curves representing equilibrium among minerals, vapor, and liquid that are not apparent in the corresponding curves for coexisting minerals and a single fluid phase. Note also that the solubilities of calc-silicate minerals are increased significantly in the liquid phase at high NaCl concentrations.

Fig. 13. Temperature–N_{CO_2} diagram depicting mineral–fluid equilibria in the system CaO–MgO–SiO_2–H_2O–CO_2–NaCl at 2 kbar along parabinary PA-3 in Fig. 6B. The dashed curve represents the limits of the miscibility gap in the system H_2O–CO_2–NaCl (see text and caption of Fig. 8).

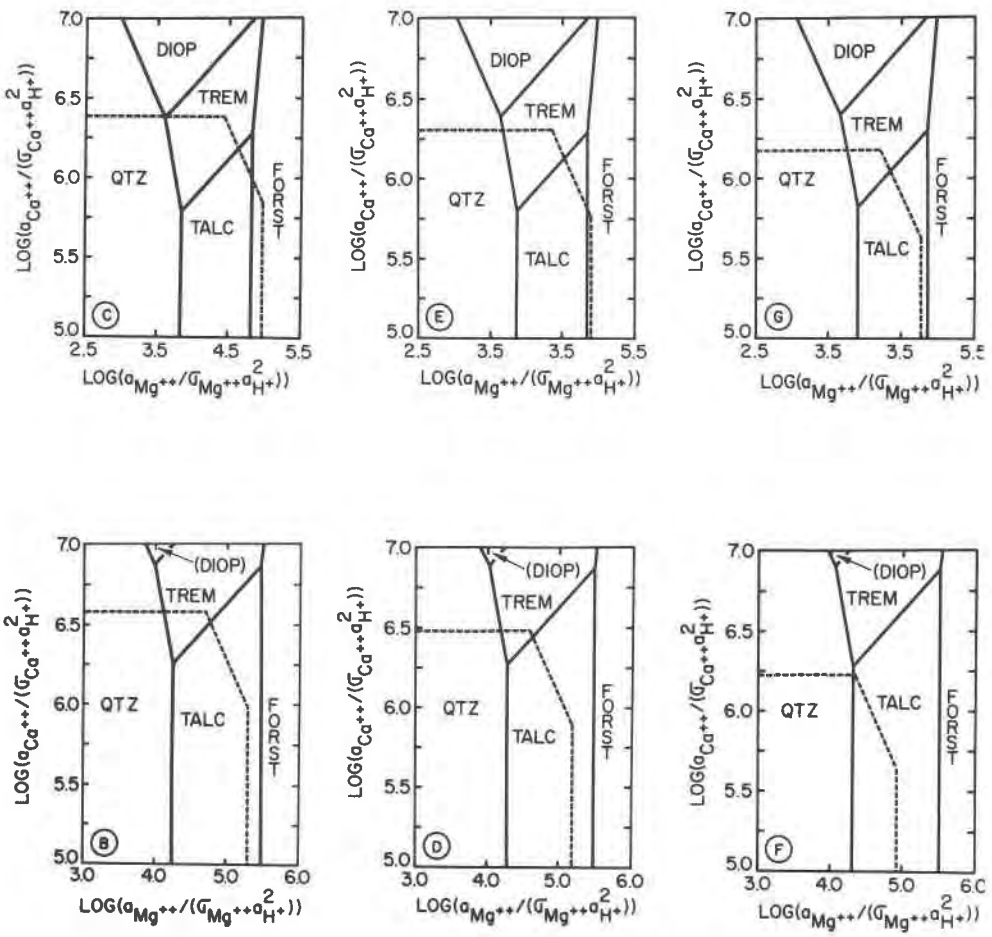

Fig. 14. Logarithmic activity diagrams for the system CaO–MgO–SiO_2–H_2O–CO_2–NaCl at 2 kbar. The circled letters in the lower left corners of the diagrams refer to the temperatures and fluid compositions with corresponding labels in Figures 8, 12, and 13 (see text). The dashed lines represent fluid saturation with respect to calcite (horizontal lines), magnesite (vertical lines), and dolomite (diagonal lines).

Concluding remarks

The results of calculations summarized above leave little doubt that metamorphic phase equilibria may be highly sensitive to X_{NaCl} in the fluid. The phase diagrams discussed in the preceding pages representing equilibrium among minerals and a single fluid phase or coexisting liquid and vapor phases in the system H_2O–CO_2–NaCl illustrate but a few examples of the dramatic consequences of nonideality and immiscibility in multicomponent crustal fluids on mineral relations in geologic systems. Many mineral assemblages that are stable in the presence of a fluid over a narrow range of composition in the binary system H_2O–CO_2 may coexist with fluids that exhibit a wide range of composition in the ternary system H_2O–CO_2–NaCl, and vice versa. The fact that separation of a liquid and vapor from a single fluid phase in the ternary system can occur at pressures and temperatures in excess of 2 kbar and 550°C suggests that immiscibility may be responsible for apparent contradictions between phase relations documented by experiments with fluids in the system H_2O–CO_2 and those observed in metamorphic rocks.

Highly saline solutions may be generated from NaCl-poor fluids as a result of immiscibility. For example, decreasing temperature and/or pressure to 500°C and 500 bars will result in unmixing of a fluid in which $X_{CO_2} = 0.2$, $X_{NaCl} = 0.04$, and $X_{H_2O} = 0.76$ to 14 mole% liquid in which $X_{CO_2} = 0.004$, $X_{NaCl} = 0.18$ (~12 molal), and $X_{H_2O} = 0.816$ coexisting with 86 mole% vapor in which $X_{CO_2} = 0.735$, $X_{NaCl} = 0.016$, and $X_{H_2O} = 0.249$. This process affords an alternative mechanism to those proposed in the past to explain the origins of highly saline fluids in diverse geologic environments. These include partitioning of chlorine gas and chloride complexes of alkalies, alkaline earths, and heavy metals into a magmatic aqueous phase generated by retrograde boiling during cooling of a hydrous magma at intermediate pressures (Burnham and

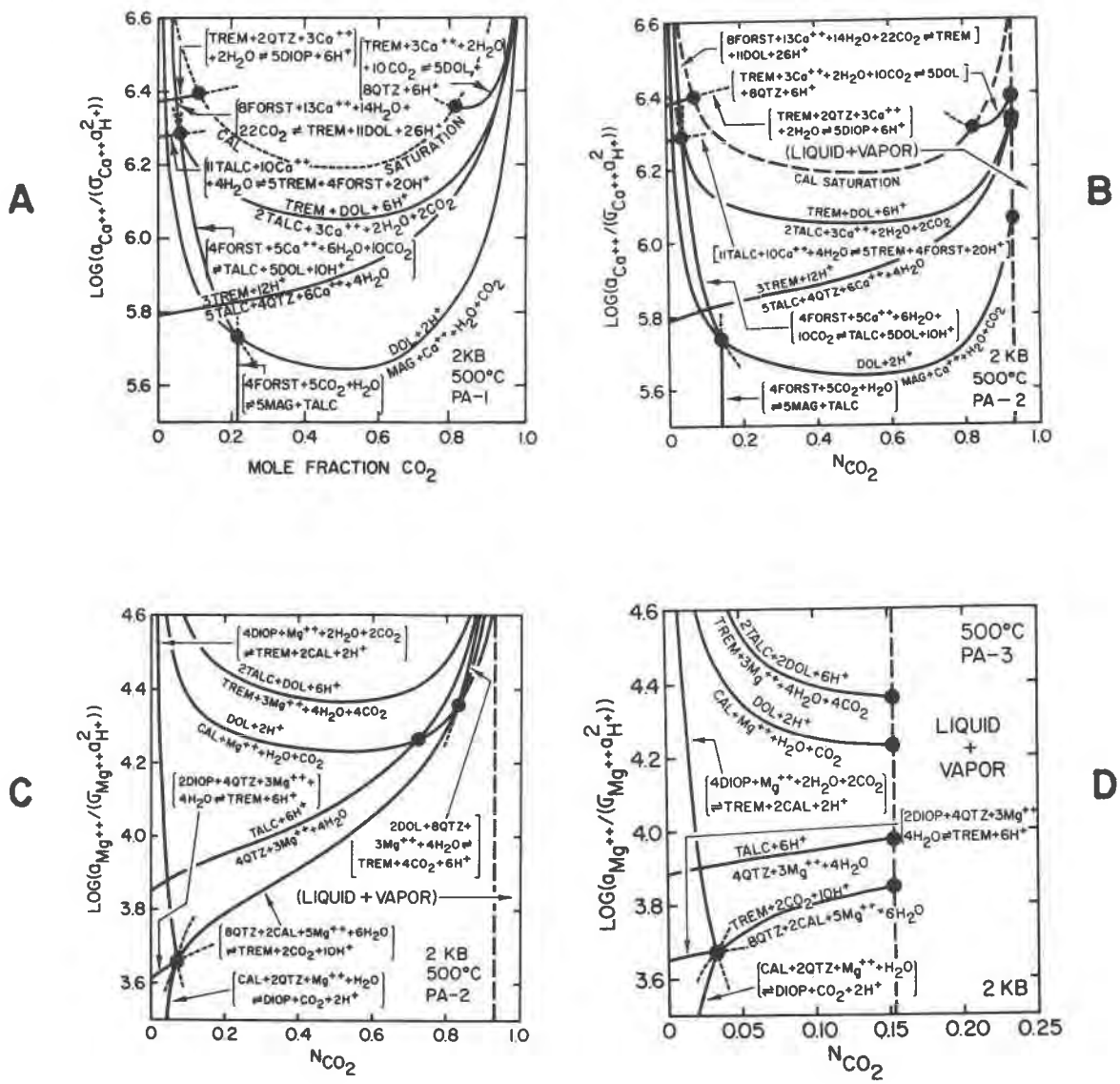

Fig. 15. $\log(a_{Mg^{++}}/(\sigma_{Mg^{++}}a_{H^+}^2))$ and $\log(a_{Ca^{++}}/(\sigma_{Ca^{++}}a_{H^+}^2))$ at 2 kbar and 500°C as a function of X_{CO_2} and N_{CO_2} in fluids coexisting with minerals in the system CaO–MgO–SiO_2–H_2O–CO_2–NaCl along the binary and parabinaries designated as PA-1, PA-2, and PA-3 in Fig. 6B (see text). The long-dash curves in diagrams B, C, and D represent the limits of the miscibility gap in the system H_2O–CO_2–NaCl.

Ohmoto, 1980). It has also been proposed that highly saline fluids found in the pore spaces of sandstones may have been derived from evaporites, or by filtration through semipermeable shale membranes (Hunt, 1979; Kharaka and Smalley, 1976).

Although the results of the calculations summarized above apply to fugitive phases in the system H_2O–CO_2–NaCl, they are probably indicative of the consequences of reactions among minerals and coexisting liquid and vapor or fluid phases involving H_2O, CO_2, and substantial concentrations of other electrolytes such as KCl, $MgCl_2$, or $CaCl_2$. Many more experimental studies will be required to assess adequately the effects of these electrolytes on devolatilization reactions. In the interim, calculations of the kind described above should afford close approximation of metamorphic phase relations as a function of X_{NaCl} and N_{CO_2} at high pressures and temperatures.

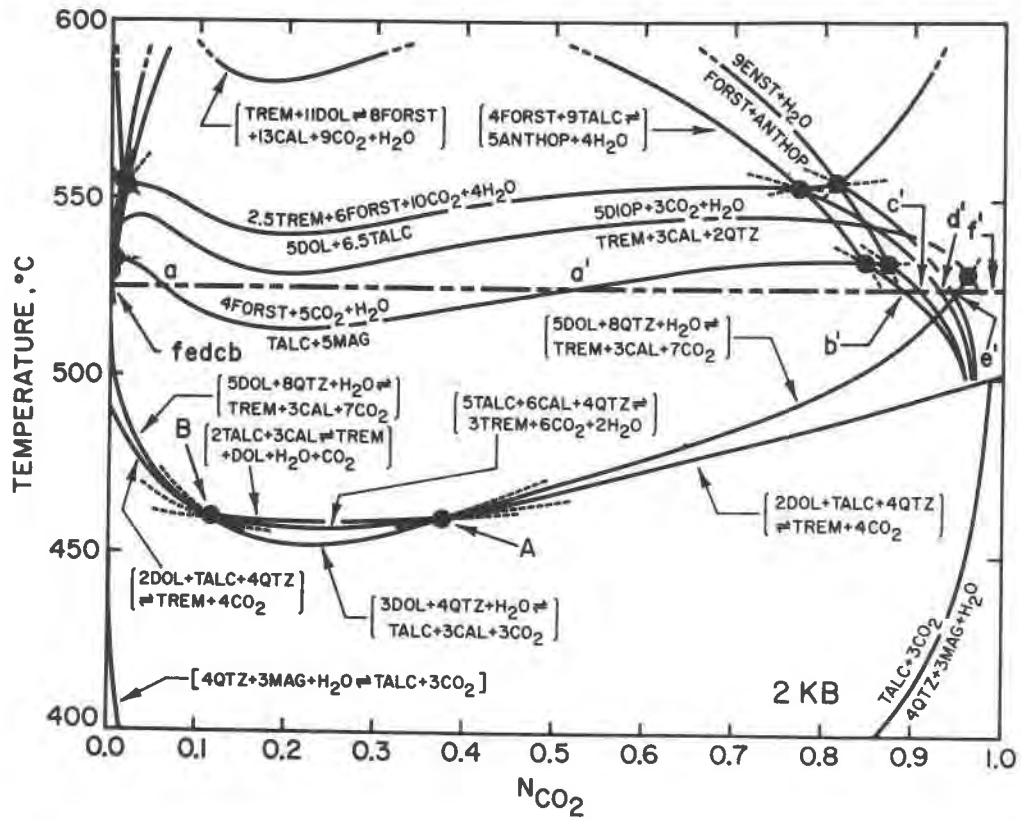

Fig. 16. Temperature–N_{CO_2} diagram depicting mineral–fluid equilibria in the system CaO–MgO–SiO_2–H_2O–CO_2–NaCl in the two-phase liquid + vapor region of the subsystem H_2O–CO_2–NaCl at 2 kbar (see text). The double-short-dash long-dash horizontal line corresponds to the trace of the cross-section represented by the large triangular diagram in Fig. 17, which is labeled with the same lower case letters shown above.

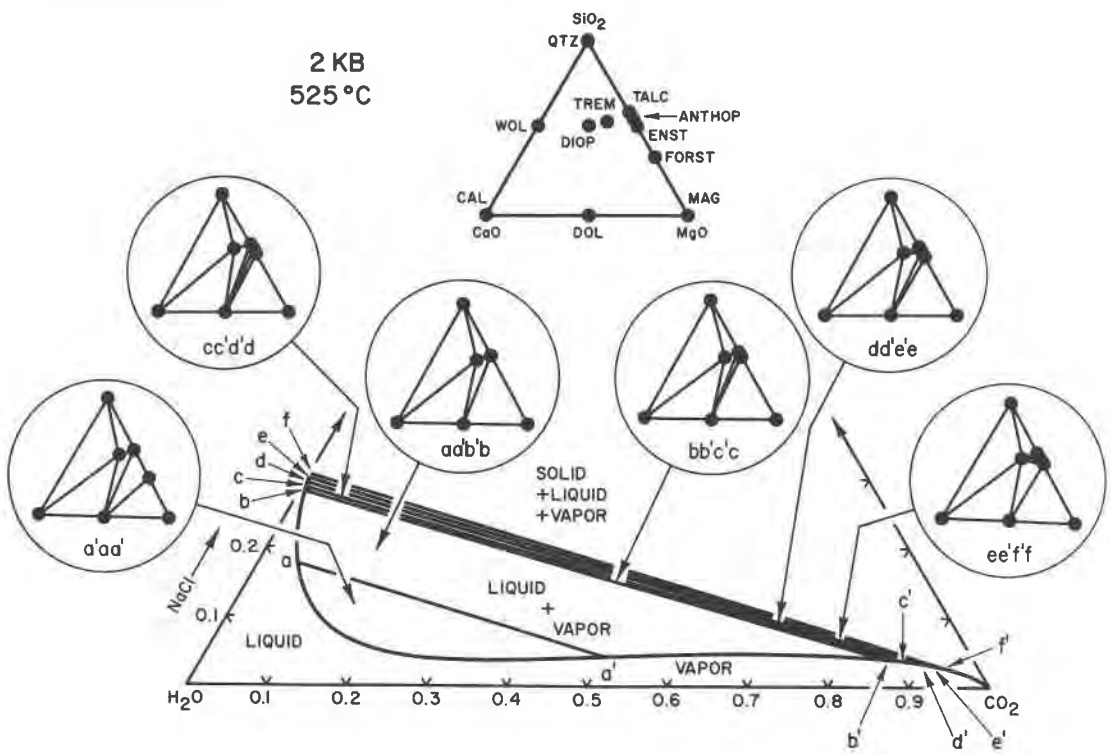

Fig. 17. Cross section of the ternary system H_2O–CO_2–NaCl at 2 kbar and 525°C (large triangle) along the horizontal line labeled *ff'* in Fig. 16. The letters shown within the large circles designate the limits in the large triangle of the compositional range of liquid + vapor for which the mineral assemblages shown in the circled triangles are stable (see text).

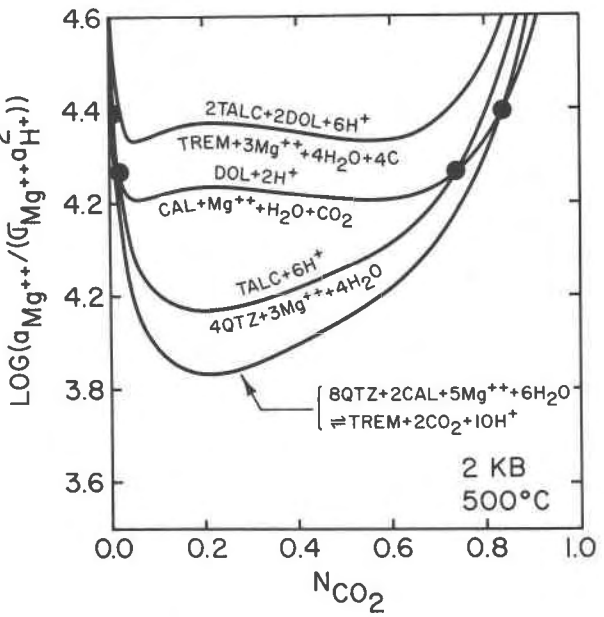

Fig. 18. Log $(a_{Mg^{++}}/(\sigma_{Mg^{++}}a^2_{H^+}))$ as a function of N_{CO_2} for mineral–fluid equilibria in the system CaO–MgO–SiO_2–H_2O–CO_2–NaCl in the two-phase liquid + vapor region of the subsystem H_2O–CO_2–NaCl at 2 kbar and 500°C (see text).

Acknowledgments

The research reported above represents the second part of the senior author's Ph.D. dissertation at the University of California, Berkeley. We are indebted to George C. Flowers, R. Miki Moore, Carol J. Bruton, Kenneth J. Jackson, Everett L. Shock, William M. Murphy, John C. Tanger IV, Peter C. Lichtner, Richard O. Sack, Mark S. Ghiorso, Cathy J. Wilson, Dara Gilbert, Michael J. O'Leary, Tom Welsh, Laurel B. Goodwin, Mary Gilzean, Joachim Hampel, Mike Ryan, Greg Williams, Korda Cordes, Joan Bossart, Mark L. Bowers, John A. Smegal, and others among our friends and colleagues at Berkeley for helpful suggestions, assistance, and encouragement during the course of this research. Thanks are also due E. Ulrich Franck and the members of the Institut für Physikalische Chemie und Elektrochemie der Universität Karlsruhe in Germany for their hospitality, assistance, and stimulating discussions during a five-month stay by one of us (T.S.B.). The research project was supported by the National Science Foundation (NSF grants EAR 77-14492 and EAR 81-15859) and the Committee on Research at the University of California, Berkeley. Finally, we would like to express our appreciation to George H Brimhall, John M. Prausnitz, John R. Holloway, and John M. Ferry for their constructive reviews of the manuscript and helpful suggestions for improvement.

References

Barton, P. B., Jr., Bethke, P. M., and Roedder, E. (1977) Environment of ore deposition in the Creede mining district, San Juan Mountains, Colorado: Part III. Progress toward interpretation of the chemistry of the ore-forming fluid for the OH vein. Economic Geology, 72, 1–24.

Bowers, T. S. and Helgeson, H. C. (1983) Calculation of the thermodynamic and geochemical consequences of nonideal mixing in the system H_2O–CO_2–NaCl on phase relations in geologic systems: Equation of state for H_2O–CO_2–NaCl fluids at high pressures and temperatures. Geochimica et Cosmochimica Acta, 47, 1247–1275.

Burnham, C. W. and Ohmoto, H. (1980) Late-stage processes of felsic magmatism. Mining Geology Special Issue, No. 8, 1–11.

Crawford, M. L., Kraus, D. W., and Hollister, L. S. (1979) Petrologic and fluid inclusion study of calc-silicate rocks, Prince Rupert, British Columbia. American Journal of Science, 9, 1135–1159.

Gehrig, M. (1980) Phasengleichgewichte und PVT-Daten ternärer Mischungen aus Wasser, Kohlendioxide, und Natriumchlorid bis 3 kbar and 550°C. Doctoral dissertation, University of Karlsruhe, Hochschulverlag, Freiburg.

Helgeson, H. C. and Kirkham, D. H. (1974) Theoretical prediction of the thermodynamic behavior of aqueous electrolytes at high pressures and temperatures: I. Summary of the thermodynamic/electrostatic properties of the solvent. American Journal of Science, 274, 1089–1198.

Helegson, H. C., Kirkham, D. H., and Flowers, G. C. (1981) Theoretical prediction of the thermodynamic behavior of aqueous electrolytes at high pressures and temperature. IV. Calculation of activity and osmotic coefficients and apparent molal and standard and relative molal properties to 600°C and 5 kb. American Journal of Science, 281, 1249–1493.

Helgeson, H. C., Delany, J. M., Nesbitt, H. W., and Bird, D. K. (1978) Summary and critique of the thermodynamic properties of rock-forming minerals. American Journal of Science, 278A, 229 p.

Hendel, E. M. and Hollister, L. S. (1981) An empirical solvus for CO–H_2O–2.6 wt % salt. Geochimica et Cosmochimica Acta, 45, 225–228.

Hollister, L. S. and Burruss, R. C. (1976) Phase equilibria in fluid inclusions from the Khtada Lake metamorphic complex. Geochimica et Cosmochimica Acta, 40, 163–175.

Hunt, J. M. (1979) Petroleum Geochemistry and Geology. W. H. Freeman and Co., San Francisco.

Jacobs, G. K. and Kerrick, D. M. (1981) Devolatilization equilibria in H_2O–CO_2 and H_2O–CO_2–NaCl fluids: an experimental and thermodynamic evaluation at elevated pressures and temperatures. American Mineralogist, 66, 1135–1153.

Kharaka, Y. K. and Smalley, W. C. (1976) Flow of water and solutes through compacted clays. American Association of Petroleum Geologists Bulletin, 60, 973–980.

Kreulen, R. (1980) CO_2-rich fluids during regional metamorphism on Naxos (Greece): carbon isotopes and fluid inclusions. American Journal of Science, 280, 745–771.

Leroy, J. and Poty, B. (1969) Recherches préliminaires sur les fluides associés à la genèse des minéralisations en uranium du Limousin (France). Mineralium Deposita, 4, 395–400.

Lyakhov, Y. V. and Popivnyak, I. V. (1978) Physiochemical conditions of development of gold mineralization in Northern Buryatia. International Geology Review, 20, 955–967.

Petrovskaya, N. V., Elinson, M. M., and Nikolayeva, L. A. (1973) Composition and conditions of formation for gas inclusions in native gold. Manuscript, 9p.

Poty, B. P., Leroy, J., and Cuney, M. (1974) Les inclusions fluides dans les minerais des gisements d'uranium intragranitiques du Limousin et du Forez (Massif Central, France), in Formation of Uranium Ore Deposits, Proceedings, International Atomic Energy Agency, Vienna, 569–582.

Roedder, E. and Coombs, D. S. (1967) Immiscibility in granitic melts, indicated by fluid inclusions in ejected granitic blocks from Ascension Island. Journal of Petrology, 8, 417–451.

Roedder, E. (1971) Fluid inclusion studies on the porphyry type ore deposits at Bingham, Utah, Butte, Montana, and Climax, Colorado. Economic Geology, 66, 98–120.

Sisson, V. B., Crawford, M. L., and Thompson, P. H. (1981) CO_2-brine immiscibility at high temperatures, evidence from calcareous metasedimentary rocks. Contributions to Mineralogy and Petrology, 78, 371–378.

Walther, J. V. and Helgeson, H. C. (1980) Description of metasomatic phase relations at high pressures and temperatures: 1. Equilibrium activities of ionic species in nonideal mixtures of CO_2 and H_2O. American Journal of Science, 280, 575–606.

Manuscript received, August 27, 1982;
accepted for publication, April 25, 1983.